Silicide formation and structural evolution in Fe-, Co-, and Ni-implanted silicon

Zhengquan Tan*
Brookhaven National Laboratory, Upton, New York 11973
and Physics Department, University of Connecticut, Storrs, Connecticut 06269-3046

F. Namavar
Spire Corporation, Bedford, Massachusetts 01730-2396

J. I. Budnick, F. H. Sanchez, and A. Fasihuddin
Physics Department, University of Connecticut, Storrs, Connecticut 06269-3046
and Institute of Materials Science, University of Connecticut, Storrs, Connecticut 06269-3046

S. M. Heald
Brookhaven National Laboratory, Upton, New York 11973

C. E. Bouldin and J. C. Woicik
National Institute of Standards and Technology, Gaithersburg, Maryland 20899
(Received 6 June 1991; revised manuscript received 30 December 1991)

Silicide formation and structural evolution in Fe-, Co-, and Ni-implanted silicon have been studied with use of extended x-ray-absorption fine-structure, x-ray-diffraction, and Rutherford backscattering spectrometry. Si(100) wafers were implanted at elevated temperatures, typically 350 °C, to doses ranging from 1×10^{16} to 1×10^{18} ions/cm^2. In the Co-implanted system, $CoSi_2$ forms with doses as low as 1×10^{16} Co/cm^2 and up to 3×10^{17} Co/cm^2, where the CoSi phase starts to form. At higher doses (8×10^{17} Co/cm^2), ordered CoSi and a CoSi-like short-range-ordered phase coexist. The silicide formation observed in the Ni-implanted system is similar to that in the cobalt-implanted system. In the case of iron implantation, Fe is coordinated with about eight Si atoms in the $(1\text{–}3)\times10^{17}$ Fe/cm^2 range as in the tetragonal $FeSi_2$. However, the $FeSi_2$ phase forms only at around 5×10^{17} Fe/cm^2. At even higher doses, a substantial amount of iron is in disordered states in addition to the ordered FeSi phase. Upon annealing at 900 °C, semiconducting β-$FeSi_2$ forms in all the Fe-implanted samples independent of the dose. Mechanisms for silicide formation in these ion-implanted systems are discussed with respect to crystal structure, diffusion, and implantation damage.

I. INTRODUCTION

It has been demonstrated that implantation of metals into silicon produces various silicides.[1–7] In particular, silicide formation and synthesis of silicide-silicon heterojunctions in the cobalt-implanted system have been studied quite extensively.[8–17] The silicide formation in ion-implanted material exhibits characteristics that differ from solid-state thermal reactions. For example, when cobalt is implanted in silicon, buried $CoSi_2$ forms at relatively low doses and CoSi forms only at high doses.[8,9,13] In contrast, upon annealing the layered Co-Si system, the metal-rich silicide Co_2Si and CoSi phases form at temperatures lower than those required for the $CoSi_2$ formation.[18,19] Epitaxial $CoSi_2$ fully aligned (type A) with Si(100) has been achieved by ion implantation plus thermal annealing.[10–12] In solid-state reaction, both type-A and type-B (rotated by 180°) orientations are present. Several recent studies dealt with the cobalt silicide growth upon post-implantation annealing.[3,5,10–16] Silicide formation in the as-implanted materials is less known, especially in very-high-dose implants. We shall demonstrate in this paper that the silicide formation in the as-implanted samples is complex and generally differs from that in the annealed samples. The as-implanted material is important for studying the ion-beam interaction with the silicon matrix and silicides.

In order to understand silicide formation in the implanted systems, we have carried out extensive x-ray-absorption fine-structure (EXAFS) measurements on the Fe-, Co-, and Ni-implanted Si(100). The EXAFS study is complemented with x-ray diffraction (XRD) and Rutherford backscattering spectrometry (RBS) experiments. Because the EXAFS technique is capable of probing the local environment around the implanted metal species and is sensitive to both short- and long-range-ordered phases, we are able to detect the silicide phases formed at the early stages and follow the structural evolution as the implant dose increases. We will discuss the silicide formation and structural evolution in these systems in terms of silicide crystal structure, the diffusion process, and implantation damage.

II. EXPERIMENTS AND DATA ANALYSIS

Polished silicon (100) wafers were uniformly implanted with a scanning ion beam at energies of 150 and 165 keV

in a vacuum better than 10^{-6} Torr at the University of Connecticut and also at Spire Corporation. Current densities of 10–20 μA/cm^2 were used to obtain nominal total doses in the range of 1×10^{16} to 1×10^{18} ion/cm^2. The Si(100) substrates were firmly attached to a sample holder using silver paint and were implanted at 400 °C, 350 °C, 100 °C, and room temperature, respectively. The results presented below are for the 350 °C implanted sample unless otherwise specified. Some samples were isothermally annealed at 700 °C or 900 °C for 2 h in a N_2 atmosphere.

The EXAFS measurements were carried out on beam lines X-11A and X-23A2 at the National Synchrotron Light Source (NSLS). The x-ray storage ring was operated at 2.5 GeV and 110–230 mA. At beam line X-11A, a Si(111) double-crystal monochromator with a 0.5-mm entrance slit was used and the energy resolution at the Co K edge is estimated to be 2.0 eV. Harmonics were rejected by detuning the crystals to reduce 20% of the peaked incident intensity. EXAFS spectra of implanted samples were measured by a fluorescence method using an ionization chamber and filter-slits assembly.[20] Bragg diffraction peaks from the Si(100) substrate were avoided by adjusting the x-ray incident angle on the sample and selectively blocking the diffracted beam in front of the detector. The filter also reduced the diffracted beam intensity. At beam line X-23A2, a Si(220) double-crystal monochromator with a 2-mm entrance slit was employed. The fluorescence signal was detected using a silicon-photodiode detector without filters. EXAFS spectra were also acquired for bulk silicides, including powdered FeSi, $FeSi_2$, $CoSi_2$, $NiSi_2$, thin-film CoSi, and NiSi on silicon substrates, as well as Fe, Co, and Ni foils. The commercially obtained bulk silicides came with a 99.9% purity grade and were checked by powder x-ray diffraction. The $FeSi_2$ powder consisted mainly of the orthorhombic β phase plus a small amount of the tetragonal α phase. All EXAFS measurements were made at room temperature, except that the 7.5×10^{17} and 8.0×10^{17} Co/cm^2 samples were measured at about 80 K in a liquid-nitrogen Dewar.

X-ray-diffraction measurements were undertaken using a θ-2θ diffractometer and a Read camera employing Cu $K\alpha$ radiation. To give a rough idea of the sensitivity of our θ-2θ XRD experiments, we note that the (400) reflection of $CoSi_2$ in the 700 °C annealed 1×10^{17} Co/cm^2 sample is 100 times stronger than the background. Rutherford backscattering experiments were performed on a 2-MeV Van de Graaff Accelerator at the University of Connecticut using a 1.9-MeV $^4He^+$ beam. The beam incident angle was about 10° with respect to the normal of the sample surface and channeling effect was minimized. The energy was calibrated by measuring backscattering of a gold film and bulk silicon. The metal concentration profile was calculated from the RBS data assuming that the sample density is a linear combination of the bulk atomic density of Si and the metal. The effects of the energy straggling and the finite detector resolution were not corrected for.

EXAFS data were analyzed with the University of Washington analysis package using a formalism based on single-scattering theory.[21] The EXAFS function is normalized to the edge jump. Figure 1 presents the EXAFS spectra for selected Co-implanted samples. The first- and second-shell contributions were Fourier-transform filtered and analyzed by a combination of log ratio and nonlinear least-squares fitting. The reference backscattering and phase-shift values were extracted from compounds of known structures. The Ni-Ni pair in nickel metal and the Ni-Si pair in $NiSi_2$ were used for the Ni-implanted samples. The Co-Co pair in cobalt metal (hexagonal-close-packed structure) and the Co-Si pair in $CoSi_2$ were used for the corresponding pairs in the Co implants. Since direct Fe-Fe and Fe-Si references are not available, the Co-Co and Co-Si pairs were also used as an approximation for Fe-Fe and Fe-Si pairs, respectively, in the iron-implanted samples. The reliability of this approximation was tested by fitting the Fe EXAFS spectra of bulk $FeSi_2$, FeSi, and Fe metal. Such a fitting analysis gave parameters that match their known values. Fitting the EXAFS data of selected Fe-implanted samples using the theoretically calculated amplitude and phase[22] resulted in parameters that agree with those obtained using Co-Co and Co-Si standards. The structural parameters obtained from fitting are listed in Table I. The $\Delta\sigma^2$ value is relative to the σ^2 of the reference pair. The uncertainty quoted in parentheses was obtained from the variation of the parameter that gives twice the minimum residue ($2\chi^2$). To take into account the correlation between the edge energy (E_0) and near-neighbor distance (R), and between the coordination number (N) and the Debye-Waller factor, these pairs for a given shell were allowed to vary simultaneously from their optimum values. The coordination number and near-neighbor distance around the metal atom in relevant silicides are listed in Table II, and serve as the standard for identifying the silicide phases in the implanted material.

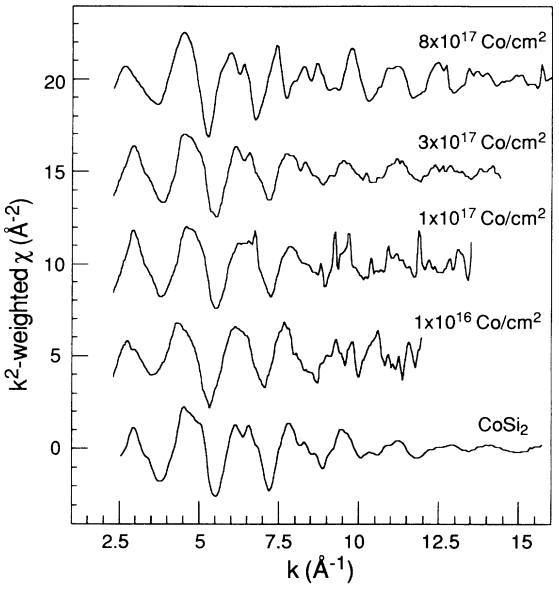

FIG. 1. Co K-edge EXAFS spectra (weighted by k^2) of Co-implanted Si(100) and bulk $CoSi_2$. The 1×10^{17} Co/cm^2 sample was implanted at 400 °C and the others at 350 °C.

III. RESULTS

A. Cobalt-implanted Si(100)

We have extended our earlier studies[8,9] of the Co-implanted system to a lower dose, i.e., 1×10^{16} Co/cm^2. We will discuss the results only to the extent sufficient for comparison with the Fe- and Ni-implanted systems and refer to our previous reports for further details. Figure 2 displays the cobalt concentration profile deduced from the RBS data for the 1×10^{17}, 3×10^{17}, and 8×10^{17} Co/cm^2 samples. Co atoms in the 1×10^{17} Co/cm^2 sample are buried. However, large amounts of Co appear near the surface and are almost uniformly distributed in the top 1000 Å in the 3×10^{17} and 8×10^{17} Co/cm^2 samples. The Co concentration approaches a saturation limit near 8×10^{17} Co/cm^2. Particularly interesting is a clear cobalt migration from the surface toward high concentration region in the annealed 1×10^{17} Co/cm^2 sample. This corresponds to the growth of large $CoSi_2$ crystallites that are fully aligned with the the silicon (100) substrate as observed by cross-sectional transmission electron microscopy (TEM) and electron diffraction. Annealing the higher-dose samples also leads to the formation of monocrystalline $CoSi_2$. Similar results are also documented in the literature.[10–16]

TABLE I. Structural parameters, determined by fitting the Co, Ni, and Fe EXAFS data, for the first and second coordination shells around the metal in the ion-implanted samples.

Sample	Neighbor	R (Å)	N	$\Delta\sigma^2$ (Å^2)	XRD
1×10^{16} Co/cm^2	Si	2.36(2)	6.2(2.2)	−0.004(4)	none
1×10^{17} Co/cm^2	Si	2.32(2)	8.1(1.2)	0.000(2)	none
3×10^{17} Co/cm^2	Si	2.32(1)	7.4(1.2)	0.000(2)	$CoSi_2$
	Co	2.69(4)	1.5(1.2)	0.000(5)	CoSi
7.5×10^{17} Co/cm^2 (80 K)	Si	2.34(1)	7.5(0.8)	0.003(2)	CoSi
	Co	2.74(2)	3.0(0.3)	−0.005(1)	
8×10^{17} Co/cm^2 (80 K)	Si	2.36(2)	8.2(1.4)	0.003(2)	none
	Co	2.74(2)	3.1(0.4)	−0.006(1)	
1×10^{17} Ni/cm^2	Si	2.35(2)	8.7(1.4)	−0.002(2)	none
3×10^{17} Ni/cm^2	Si	2.35(2)	8.9(0.8)	0.000(1)	$NiSi_2$(?)
	Ni	2.82(3)	2.4(1.7)	0.003(6)	
8×10^{17} Ni/cm^2	Si	2.34(2)	8.0(0.8)	0.001(1)	none
	Ni	2.65(4)	2.2(1.2)	0.001(4)	
1×10^{17} Fe/cm^2	Si	2.30(3)	7.4(1.3)	0.006(3)	none
3×10^{17} Fe/cm^2	Si	2.36(2)	8.9(1.2)	0.004(2)	none
5×10^{17} Fe/cm^2	Si	2.35(2)	5.8(1.2)	−0.0009(16)	FeSi
	Fe	2.71(3)	2.5(1.3)	0.0010(43)	
	Fe	2.98(7)	0.7(0.6)	0.0017(11)	
$FeSi_2$ powder	Si	2.35(1)	7.2(0.8)	0.0006(10)	β-$FeSi_2$
	Fe	2.70(2)	1.3(0.6)	−0.0021(12)	α-$FeSi_2$
	Fe	2.96(3)	1.4(0.3)	0.0014(30)	
7×10^{17} Fe/cm^2	Si	2.33(2)	5.5(1.4)	0.003(3)	FeSi
	Fe	2.74(2)	2.7(0.6)	−0.004(1)	
8×10^{17} Fe/cm^2	Si	2.33(2)	4.7(1.1)	0.003(3)	FeSi
	Fe	2.75(2)	1.8(0.4)	−0.004(1)	
1×10^{18} Fe/cm^2	Si	2.34(2)	3.1(0.5)	0.000(1)	FeSi
	Si	2.46(10)	1.4(0.7)	0.036(98)	Fe_5Si_3
	Fe	2.72(2)	2.3(0.7)	−0.002(1)	
6.55×10^{17} Fe/cm^2 (900 °C, 2 h)	Si	2.34(3)	7.9(1.1)	−0.0006(11)	β-$FeSi_2$
	Fe	2.95(3)	2.0(1.4)	−0.0028(39)	

TABLE II. Radial distribution around the metal atom in selected transition-metal silicides. Data are listed as groups of the near-neighbor number, type, and distance in angstroms. [The crystallographic data used here were taken from P. Villars and L. D. Calvert, *Pearson's Handbook of Crystallographic Data for Intermetallic Phases* (American Society for Metals, Metals Park, 1985).]

Cubic $CoSi_2$ ($a=5.365$ Å)			Cubic $NiSi_2$ ($a=5.406$ Å)			Tetragonal $FeSi_2$ ($a=2.695$ Å, $c=5.134$ Å)		
8	Si	2.323	8	Si	2.341	8	Si	2.357
12	Co	3.794	12	Ni	3.823	4	Fe	2.695
24	Si	4.450	24	Si	4.482	4	Fe	3.811
						8	Si	4.204
Cubic CoSi ($a=4.460$ Å)			**Cubic NiSi ($a=4.446$ Å)**			**Cubic FeSi ($a=4.489$ Å)**		
1	Si	2.294	1	Si	2.287	1	Si	2.309
3	Si	2.338	3	Si	2.331	3	Si	2.353
3	Si	2.478	3	Si	2.471	3	Si	2.495
6	Co	2.738	6	Ni	2.729	6	Fe	2.756
3	Si	3.652	3	Si	3.641	3	Si	3.676
6	Co	4.031	6	Ni	4.018	6	Fe	4.057
3	Si	4.157	3	Si	4.144	3	Si	4.184
3	Si	4.238	3	Si	4.224	3	Si	4.265
Orthorhombic $FeSi_2$[a] ($a=9.863$ Å, $b=7.791$ Å, $c=7.833$ Å)						**Orthorhombic NiSi ($a=5.18$ Å, $b=3.34$ Å, $c=5.62$ Å)**		
Fe(1) site			Fe(2) site					
4	Si	2.338	4	Si	2.334	6	Si	2.439
4	Si	2.380	4	Si	2.433	4	Ni	2.694
2	Fe	2.967	2	Fe	2.967	2	Ni	3.340
6	Fe	3.969	2	Si	3.823	1	Si	3.499
6	Si	4.018	4	Si	3.980	1	Si	3.746
4	Fe	4.036	2	Fe	3.975	2	Si	3.923
2	Si	4.055	8	Fe	4.030	2	Ni	3.925

[a]Reference 23.

In the as-implanted samples with doses of 1×10^{17} Co/cm^2 and lower, no silicide phase can be observed in our x-ray-diffraction experiments. For the 3×10^{17} Co/cm^2 sample, three weak reflections from CoSi and a strong (400) reflection from $CoSi_2$ were identified. As the dose increases to 8×10^{17} Co/cm^2, only one weak diffraction line remains which may belong to the CoSi phase. However, the CoSi phase is identified in the 7.5×10^{17} Co/cm^2 sample implanted at 100 °C. Figure 3(a) compares the Fourier-transform magnitudes of Co EXAFS for the 1×10^{16}, 1×10^{17}, and 3×10^{17} Co/cm^2 samples with that of bulk $CoSi_2$. In the 1×10^{16} sample, the peak average Co concentration is about 1%, as derived from RBS data. To our surprise, the first coordination shell around Co in this sample is almost identical to that in bulk $CoSi_2$. On average, Co is already coordinated with an appreciable number of Co neighbors (at 3.8 Å) as in $CoSi_2$. $CoSi_2$ particles have clearly formed, even at this low dose. $CoSi_2$ remains the only significant silicide phase for doses up to about 3×10^{17} Co/cm^2. The $CoSi_2$ regions appear isolated in the silicon matrix up to 1×10^{17} Co/cm^2, since no XRD reflections of $CoSi_2$ were observed and the average Co concentration is well below that of $CoSi_2$. The EXAFS spectrum of the 3×10^{17} Co/cm^2 sample is dominated by $CoSi_2$, showing that the CoSi identified in the XRD pattern is only a minority phase. Based on the number of Co-Co bonds at 2.69(4) Å, we previously[9] estimated the molar percentage of CoSi to be 24%. The actual amount of ordered CoSi may be less than this value, since Co at the interstitial site in the

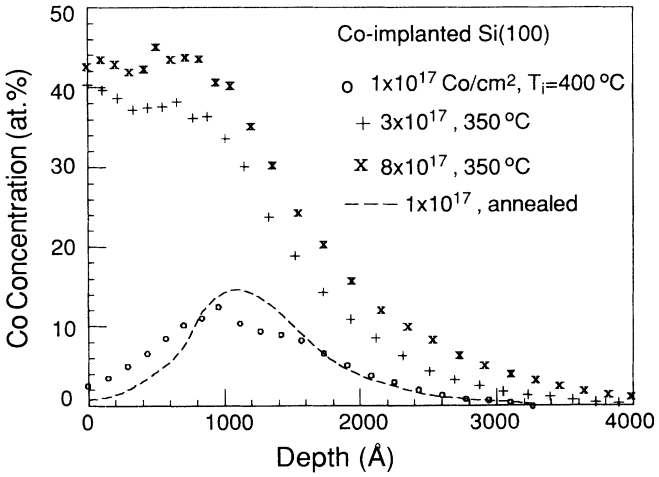

FIG. 2. The cobalt concentration profile for Co-implanted Si(100) deduced from Rutherford backscattering data.

$CoSi_2$ structure also has Co neighbors at this distance (2.68 Å, if Si neighbor positions are not distorted).

Figure 3(b) compares the Co EXAFS Fourier-transform spectrum of the 7.5×10^{17} (implanted at 100 °C) and 8×10^{17} Co/cm^2 samples with that of ordered CoSi film. The overall spectra of both samples are similar to that of CoSi. However, the fitting result indicates that Co is coordinated with eight Si at 2.34 Å and three Co at 2.74 Å, which actually differs from Co in ordered CoSi. In CoSi, the Si near neighbors are distributed at three distances, one at 2.29 Å, three at 2.33 Å, and three at 2.47 Å. In the EXAFS fitting, the 2.29- and 2.33-Å Co-Si bonds cannot be resolved. Our fitting analysis does not reveal any significant number of 2.47-Å Co-Si bonds. The Co-Si nearest-neighbor coordination is rather similar to that in $CoSi_2$, and this has been attributed to an intermediate structure via which the $CoSi_2$ evolves to CoSi in the high-dose implants.[9] In this proposed intermediate structure, the interstitial positions in the $CoSi_2$ structure are partially filled by Co atoms.[9] The bond length and coordination numbers determined from our EXAFS data rule out any significant amount of Co_2Si or Co metal clusters in the high-dose implanted samples.

B. Nickel-implanted Si(100)

The silicide formation sequence in Ni-implanted Si(100) is similar to that in the Co-implanted system.

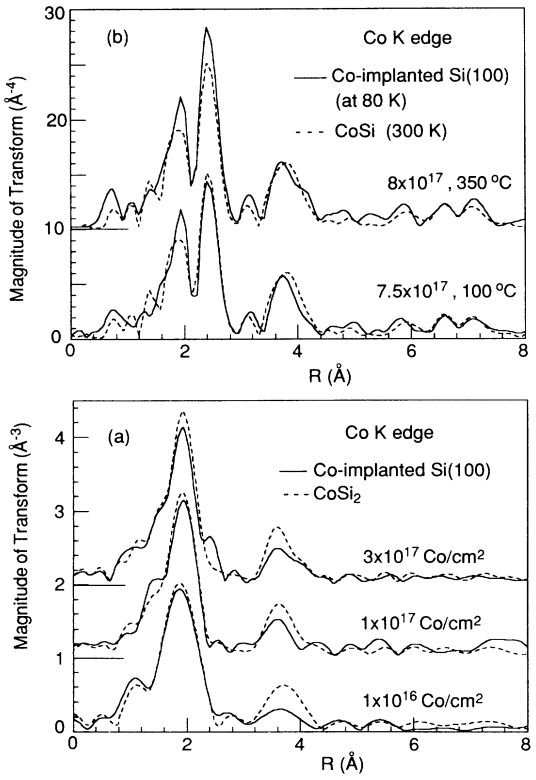

FIG. 3. Fourier-transform magnitude of Co EXAFS for Co-implanted Si(100): (a) low-dose samples compared with bulk $CoSi_2$ (dashed line). The transform k range for $CoSi_2$ was adjusted to be similar to that for each individual implanted sample. (b) High-dose samples compared with CoSi film (dashed line).

This is expected since the Ni disilicide and monosilicide have the same crystal structure as the corresponding Co silicides. The EXAFS results obtained from nonlinear least-squares fitting are summarized in Table I. As shown in Fig. 4, $NiSi_2$ is already observed at a dose of 1×10^{17} Ni/cm^2. The EXAFS amplitude is slightly larger than that in bulk $NiSi_2$, suggesting that the silicide in the implanted sample is highly ordered on a local scale. However, the silicide at this stage of implantation may still be disrupted by the unreacted silicon, since the average nickel concentration is expected to be far below that for continuous $NiSi_2$. As the dose increases to 3×10^{17} Co/cm^2, $NiSi_2$ remains the dominant silicide phase, but Ni neighbors start to appear at about 2.8 Å. At 8×10^{17} Ni/cm^2, the silicide transforms to a NiSi-like structure, Ni-Ni pairs at 2.7 Å, and 4.0 Å of the FeSi-type cubic NiSi phase are clearly observed in the implanted sample. Our EXAFS and XRD results show no evidence for the formation of the MnP-type orthorhombic NiSi, in which Ni has six Si neighbors at 2.44 Å (Table II).

C. Iron-implanted Si(100)

Figure 5 displays the Fe concentration profile in Fe-implanted Si(100). The peak concentration is about 10, 24, 40, 50, and 60 at. % for the 1, 3, 5, 7, and 10×10^{17} Fe/cm^2 samples, respectively. The retained doses (calculated from the concentration profile) in these samples are, respectively, 0.70, 1.6, 2.7, 3.4, and 3.2×10^{17} Fe/cm^2. The 30 % plateau in the 0–500-Å range for the 5×10^{17} Fe/cm^2 sample is close to the Fe concentration in $FeSi_2$. A nearly flat top of 50%, corresponding to that of FeSi, is observed in the 300–800-Å region for the 7×10^{17} Fe/cm^2 sample. In the 1×10^{18} Fe/cm^2 sample, the Fe concentration clearly peaks toward the surface, suggesting severe sputtering erosion. Differences from the Co-implanted system are noticeable. In the Fe-implanted system, the peak concentration builds up in a more gradual fashion but reaches a higher value. The Fe concentration peaks in deeper regions at low doses, but is less spread out at high doses, as compared to cobalt implants. These differences can be understood if the metal is more

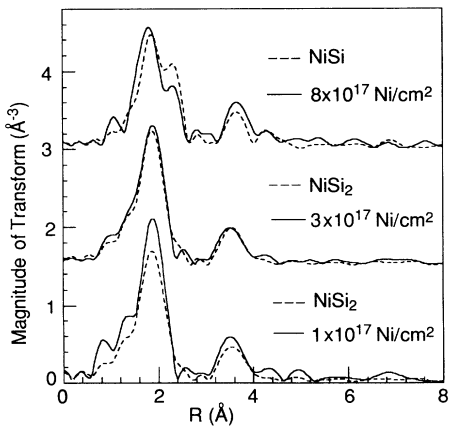

FIG. 4. Fourier-transform magnitude of Ni EXAFS for Ni-implanted Si(100) (solid line) compared with those of bulk $NiSi_2$ and a NiSi film (dashed line).

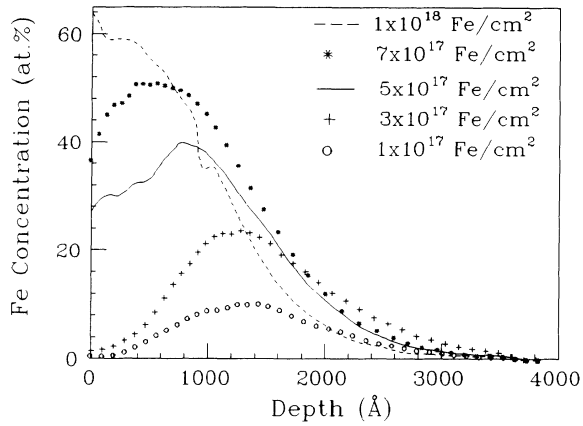

FIG. 5. Fe concentration profile for Fe-implanted Si(100) derived from RBS data.

diffusive in the Co-implanted system than in the Fe-implanted system. We will discuss these differences in more detail.

The different diffusion behavior is also reflected in the silicide formation. $CoSi_2$ forms early at 1×10^{16} Co/cm^2, but iron silicide forms only at much higher doses. Figure 6 shows the Fourier-transform spectra for Fe-implanted

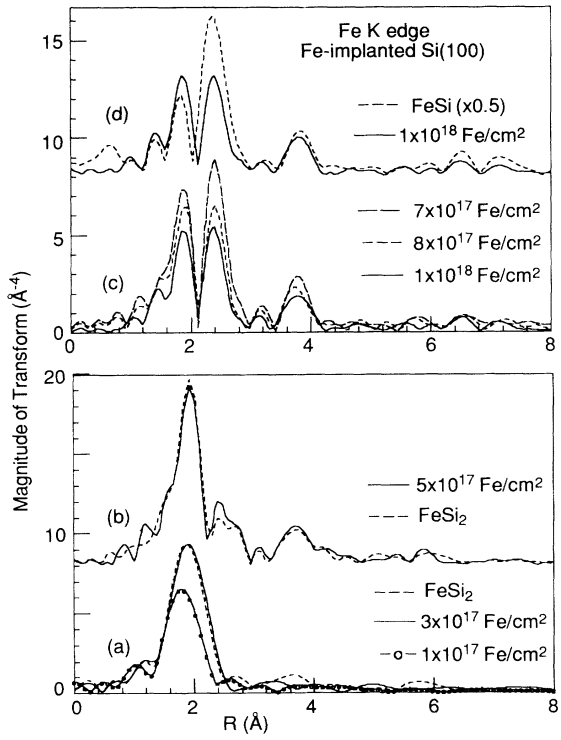

FIG. 6. Fourier-transform magnitude of Fe EXAFS ($k^3\chi$) for Fe-implanted Si(100). In (a) and (b), the low-dose samples are compared with the $FeSi_2$ powder sample (see text for details); both the lower and upper dashed curves are from the same spectrum of $FeSi_2$ but were transformed over different k ranges. (c) For high-dose samples, the EXAFS amplitudes decrease as the dose increases. (d) The 1×10^{18} Fe/cm^2 sample is compared with FeSi. Note that the FeSi spectrum is multiplied by a factor of 0.5.

samples. In the 1×10^{17} Fe/cm^2 sample, the number of Si nearest neighbors is close to 8 (Table I), indicating the ($FeSi_8$) cluster formation. However, Fe-Si pairs are relatively disordered at this stage. At 3×10^{17} Fe/cm^2, the Si nearest neighbors around Fe become more ordered, essentially the same as in the tetragonal (α-phase) $FeSi_2$. Fe-Fe neighbors expected in $FeSi_2$, however, are not identified.

$FeSi_2$ exists in two crystal structures. In the tetragonal (α) phase, metallic and stable at high temperatures, Fe has eight Si neighbors at 2.35 Å and four Fe neighbors at 2.695 Å. In the orthorhombic (β) phase, semiconducting and stable at low temperatures, Fe occupies two inequivalent sites, and on the average, each Fe has eight Si neighbors at 2.37 Å and two Fe neighbors at 2.96 Å.[23,24] Fitting analysis of the EXAFS data suggests that our $FeSi_2$ powder sample contained about 70% β phase and 30% α phase. The XRD pattern of this sample showed most of the β-phase reflections and the strong α-phase reflections. The overall spectrum of the 5×10^{17} sample is similar to that of the $FeSi_2$ powder sample [Fig. 3(b)]. The result of the fitting analysis is consistent with a combination of (63±30)% α-$FeSi_2$ and (37±30)% β-$FeSi_2$. However, a small amount of FeSi may be present and the actual amount of α-$FeSi_2$ may be less than the value indicated here. This uncertainty arises from the fact that the shortest Fe-Fe distance in α-$FeSi_2$ and that in FeSi differ by only 0.06 Å and may not be resolved in the fitting analysis. In the XRD pattern, a few weak peaks can be indexed to FeSi but no reflections from either α-$FeSi_2$ or β-$FeSi_2$ are present. Possibly, the $FeSi_2$ phases in the sample are only locally ordered and long-range order has not been established.

XRD analysis clearly identified ordered FeSi in the 7×10^{17}, 8×10^{17}, and 1×10^{18} Fe/cm^2 samples. Fe_5Si_3 may also be present in the 1×10^{18} Fe/cm^2 sample. As noted earlier, XRD detects only the long-range-ordered phase, while EXAFS probes both long- and short-range-ordered phases. A combination of the two may provide a more complete picture. Figure 6(c) shows the Fe EXAFS Fourier-transform spectra for the 7×10^{17}, 8×10^{17}, and 1×10^{18} Fe/cm^2 samples, and Fig. 6(d) compares the 1×10^{18} Fe/cm^2 sample with bulk FeSi. The overall spectral features of the implanted samples—in particular, the peak positions—resemble those of bulk FeSi. However, the EXAFS amplitudes for the implanted samples are smaller in all cases. We note that the smaller amplitude is not an artifact of the experiment such as the thickness effect. As the dose increases, the average coordination number for each Fe progressively decreases, but the pair disorder parameter ($\Delta\sigma^2$) remains about the same (Table I). We attribute the small average coordination number to the presence of Fe atoms that are in very disordered environments with minimal pair correlation. These Fe atoms absorb x rays but contribute little to the EXAFS. Reduced average coordination numbers were also observed in pure metals subjected to high-dose krypton implantation.[25]

While all near-neighbor distances identified in the implanted samples (Table I) match those of bulk cubic FeSi, the Si shell at 2.50 Å expected for ordered FeSi is not ful-

ly developed. As can be seen from Fig. 6(c), the peak in the 1.2–2.1-Å region evolves from a single-peak-like line shape at 7×10^{17} Fe/cm^2 to a split peak at 1×10^{18} Fe/cm^2; the latter is more similar to that observed in FeSi. In the least-squares fitting, inclusion of a 2.50-Å Si shell led to a vanishingly small coordination number for this shell in the 7×10^{17} Fe/cm^2 sample. In the 1×10^{18} Fe/cm^2 sample, a finite coordination number is obtained, but this shell is still not well defined, as suggested by the large disorder parameter (Table I). Figure 7 shows filtered EXAFS data and fit (dashed curve) for these two samples. The good agreement between the data and fit and, in particular, the well-reproduced beat near 8 Å^{-1} lend credibility to the parameters obtained in the fitting.

In summary, in the 1×10^{17} and 3×10^{17} Fe/cm^2 samples, we observe ($FeSi_8$) clusters that also exist in $FeSi_2$ but no clear evidence of an ordered $FeSi_2$ phase. At 5×10^{17} Fe/cm^2, both the α-$FeSi_2$ phase and the β-$FeSi_2$ phase are formed. In the 7×10^{17} to 1×10^{18} Fe/cm^2 range, ordered FeSi is formed. In addition, a substantial amount of Fe may be in very disordered environments.

The 3×10^{17} and 6.55×10^{17} Fe/cm^2 samples were also annealed in N_2 atmosphere at 900 °C for 2 h. Single-phase β-$FeSi_2$ was identified in both samples using XRD and EXAFS. Figure 8 shows the Fourier-transform EXAFS spectrum for the 6.55×10^{17} sample along with that of the as-implanted 7×10^{17} Fe/cm^2 sample. The two spectra are much different, showing the structural transformation upon thermal annealing. The distinct Fe-Fe distances in these spectra ensure unambiguous identification of the silicide phases. Synthesis of layered β-$FeSi_2$ has been demonstrated very recently.[26,27]

IV. DISCUSSION

Based on the fact that Co is coordinated with eight silicon atoms at 2.33 Å throughout the $(1-8)\times10^{17}$ Co/cm^2 range, we have proposed that the ($CoSi_8$) core acts as the nucleation center for the early $CoSi_2$ formation. As illustrated in Fig. 9(a), $CoSi_2$ consists of stacked ($CoSi_8$) cubes with every other cube missing. The identification of the ($CoSi_8$) core in the 1×10^{16} Co/cm^2 sample provides further support for this model. At a dose of 3×10^{17} Co/cm^2, the $CoSi_2$ phase is well ordered and fully aligned in the substrate orientation. This alignment is probably a result of epitaxial growth of $CoSi_2$ with the silicon matrix (the lattice mismatch between bulk $CoSi_2$ and silicon is 1.2% at room temperature). As the dose increases from 1×10^{17} to 3×10^{17} Co/cm^2, isolated $CoSi_2$ particles may coalesce to form larger grains, and the peak average Co concentration increases. This behavior is also seen in the 1×10^{17} Co/cm^2 sample upon annealing.

The next silicide phase formed is CoSi. However, the Co local environment is not exactly as in CoSi in that the 2.47-Å Co-Si bond is not fully developed. After large regions of $CoSi_2$ have formed, further implantation brings Co atoms into the $CoSi_2$. The interstitial site at the center of the $CoSi_2$ unit cell has eight Si nearest neighbors at 2.32 Å [Fig. 9(a)]. Because Co tends to bind with Si, further implanted Co atoms may prefer to occupy this in-

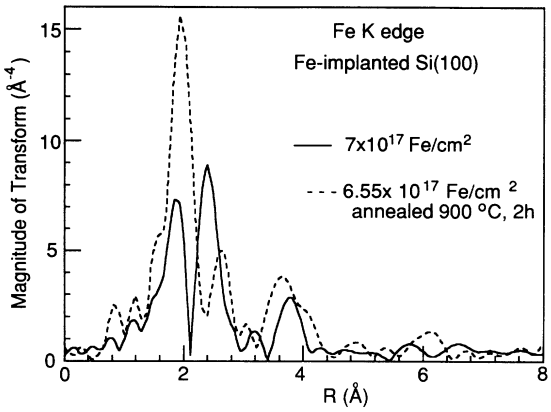

FIG. 8. Fourier-transform magnitude of Fe EXAFS ($k^3\chi$), comparing the annealed 6.55×10^{17} Fe/cm^2 and the as-implanted 7×10^{17} Fe/cm^2 samples.

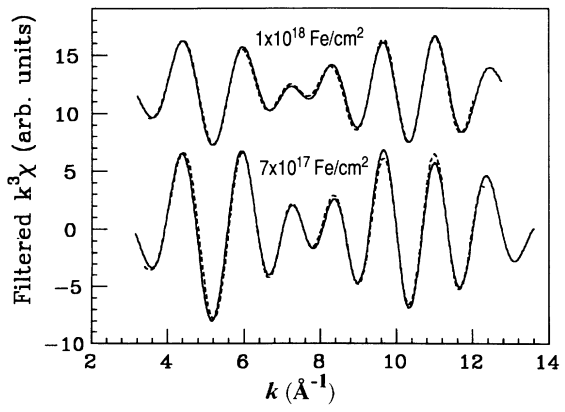

FIG. 7. Representative fits (dashed line) to Fe EXAFS data [solid line, filtered in the 1.0–3.0–Å^{-1} range in Fig. 6(c)].

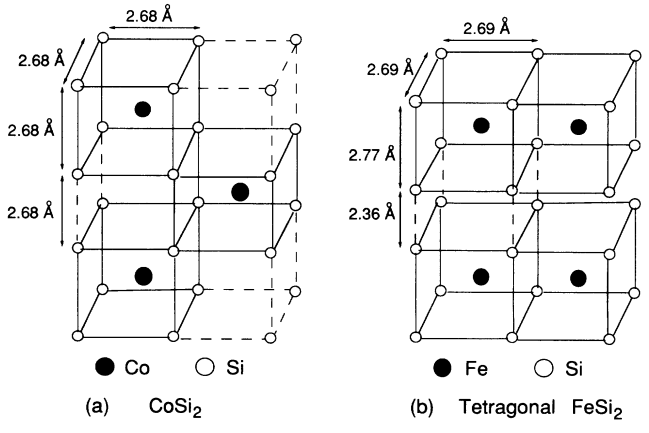

FIG. 9. Structure of (a) the fluorite-type $CoSi_2$ and (b) the tetragonal $FeSi_2$, both of which consist of (MSi_8) blocks. The blocks are stacked differently in the two structures.

terstitial site and form an intermediate defect structure, as we previously proposed.[9] This site is coordinated with eight Si atoms, as is the regular Co site of $CoSi_2$. A full occupation of the interstitial site results in a uniform Co and Si distribution and precise CoSi stoichiometry. The formation of ordered CoSi requires only local rearrangement of the Co and Si atoms from this intermediate defect structure. We believe that our EXAFS data of the 7.5×10^{17} and 8×10^{17} Co/cm^2 samples reflect a combination of the defect structure and ordered CoSi. The absence of any Co-rich silicide such as Co_2Si may partly be due to insufficient Co concentration. In addition, the Co_2Si structure is more complex than those of $CoSi_2$ and CoSi. As will be discussed shortly, complex structures are less favorable in the ion-implanted system.

In the 1×10^{17} and 3×10^{17} Fe/cm^2 samples, there is no clear indication that $FeSi_2$ forms. A ($FeSi_8$) core also forms at the early stage of Fe implantation. The lack of sufficient Fe diffusion, as suggested by the RBS data, may have delayed $FeSi_2$ formation under a dose of about 5×10^{17} Fe/cm^2, significantly higher than that required for $CoSi_2$ formation (1×10^{16} Co/cm^2). The α-$FeSi_2$ consists of ($FeSi_8$) blocks that are more densely stacked than in $CoSi_2$ (Fig. 9). Covalent Si-Si bonding (2.36 Å) and a short Fe-Fe distance (2.69 Å) are required to form $FeSi_2$. These differences in the crystal structure may also contribute to the $FeSi_2$ formation that is later than the $CoSi_2$ formation.

Interestingly, the α-$FeSi_2$ phase, stable only at high temperatures, is observed in the as-implanted 5×10^{17} Fe/cm^2 sample, while only β-$FeSi_2$ forms upon post-implantation annealing at 700–900 °C. One important difference between α-$FeSi_2$ and β-$FeSi_2$ is that the former has a much simpler crystal structure. The observation of α-$FeSi_2$ seems to suggest that phases with simple structures are favored during ion implantation. Crystalline phases formed in ion-beam mixed systems usually have simple structures.[28] In general, the phase formation can also be growth controlled. However, the growth rate may be a less important factor in the Fe-implanted Si(100) system. Since the β-$FeSi_2$ can be considered as α-$FeSi_2$ having distorted atomic positions, the Fe diffusion rate in these two structures is not likely to be sufficiently different to differentiate the growth rate of α-$FeSi_2$ and β-$FeSi_2$.

As the implant dose increases beyond the $FeSi_2$ formation, the average number of Si nearest neighbors around Fe quickly decreases from 8. An interstitial site with eight Si nearest neighbors also exists in $FeSi_2$ [Fig. 9(b)], but its distance to Si atoms (2.24 Å) is significantly shorter than the Fe-Si bond lengths found in bulk Fe silicides. An addition of Fe at this site is bound to create large distortions or even destroy the $FeSi_2$ structure. Consequently, further implanted Fe atoms may assume irregular sites or disordered positions and reduce the total EXAFS amplitude in the very-high-dose implanted samples (above 7×10^{17} Fe/cm^2). The ordered FeSi forms probably as a result of the nucleation promoted by short-range diffusion and the appropriate Fe concentration.

V. CONCLUSION

Using EXAFS combined with x-ray-diffraction and RBS techniques, we have observed silicides formed at very early stages of implantation and determined the phase evolution as the implant dose increases. During implantation, the first silicide phase to form is always the Si-rich silicide. As we have demonstrated, $CoSi_2$, $NiSi_2$, and $FeSi_2$ phases are formed initially in Co-, Ni-, and Fe-implanted Si(100), respectively. At early stages of implantation, the silicon atom supply far surpasses the metal supply. The way atoms are supplied to the reaction region largely determines the formation of the initial silicide phase. The (MSi_8) clusters form at the early stage of implantation and serve as the nucleation center for disilicide formation. As the implant dose increases, the disilicides evolve to monosilicides, CoSi, NiSi, and FeSi, but these monosilicides are not well ordered. The evolution appears to be via an intermediate structure in which the metal atoms fill the interstitial site in the cubic $CoSi_2$ and $NiSi_2$. In the very-high-dose Fe implants, a large number of Fe atoms are in disordered states, having likely resulted from implantation damage. Upon thermal annealing at 700–900 °C, $CoSi_2$, $NiSi_2$, and the β-$FeSi_2$ are formed independent of the dose.

ACKNOWLEDGMENTS

We wish to thank Dale Brewe and W. Q. Chen for assistance in the experiments. We are grateful to Dr. Q. Kessel for providing access to the Van de Graaff accelerator and to Dr. H. Hayden for help with ion implantation. Jianjun Jia is thanked for providing the CoSi and NiSi samples. We also thank Dr. P. Chartier for assistance in the x-ray-diffraction measurements. We acknowledge support from the U.S. Department of Energy, under Contract No. DE-AS05-80-ER10742 and No. DE-FG02-90ER45424. This work was carried out at beam line X-11 and X-23A2 at the National Synchrotron Light Source (NSLS), which is supported by the Department of Energy under Contract No. DE-AC02-76CH00016.

*Mailing address: Building 510E, Brookhaven National Laboratory, Upton, NY 11973.

[1]F. H. Sanchez, F. Namavar, J. I. Budnick, A. H. Fasihuddin, and H. C. Hayden, in *Beam-Solid Interactions and Phase Transformations,* edited by H. Kurz, G. L. Olson, and J. M. Poate, MRS Symposia Proceedings No. 51 (Materials Research Society, Pittsburgh, 1986).

[2]F. Namavar, F. H. Sanchez, J. I. Budnick, A. H. Fasihuddin, and H. C. Hayden, in *Beam-Solid Interactions and Transient Processes,* edited by M. O. Thomposon, S. T. Picraux, and J. S. Williams, MRS Symposia Proceedings No. 74 (Materials Research Society, Pittsburgh, 1987).

[3]A. E. White, K. T. Short, R. C. Dynes, J. Garno, and J. S. Gibson, Appl. Phys. Lett. **50**, 95 (1987).
[4]J. K. N. Lindner and E. H. te Kaat, J. Mater. Res. **3**, 1238 (1988).
[5]C. Bulle-Lieuwman, A. H. von Ommen, and L. van Ijzendoorn, Appl. Phys. Lett. **54**, 244 (1989).
[6]K. Kohlhof, S. Mantl, B. Stritzker, and W. Jager, Nucl. Instrum. Methods B **39**, 276 (1989).
[7]A. E. White, K. T. Short, R. C. Dynes, R. Hull, and J. M. Vandenberg, Nucl. Instrum. Methods B **39**, 253 (1989).
[8]Z. Tan, J. I. Budnick, F. Sanchez, G. Tourillon, F. Namavar, H. Hayden, and A. Fasihuddin, in *Synchrotron Radiation in Materials Research,* edited by J. H. Weaver, J. Gland, and R. Clarke, MRS Symposia Proceedings No. 143 (Materials Research Society, Pittsburgh, 1989).
[9]Z. Tan, J. I. Budnick, F. H. Sanchez, G. Tourillon, F. Namavar, and H. Hayden, Phys. Rev. B **40**, 6368 (1989).
[10]M. F. Wu, A. Vantomme, G. Langouche, K. Maex, H. Vanderstraeten, and Y. Bruynseraede, Appl. Phys. Lett. **57**, 1973 (1990).
[11]H. Vanderstraeten, Y. Bruynseraede, M. F. Wu, A. Vantomme, G. Langouche, and J. M. Phillips, Appl. Phys. Lett. **57**, 135 (1990).
[12]K. Maex, A. E. White, K. T. Short, Y-F. Hsieh, R. Hull, J. W. Osenbach, and H. C. Praefcke, J. Appl. Phys. **68**, 5641 (1990).
[13]R. Hull, A. E. White, K. T. Short, and J. M. Bonar, J. Appl. Phys. **68**, 1629 (1990).
[14]C. W. T. Bulle-Lieuwma, A. H. Van Ommen, D. E. W. Vandenhoudt, J. J. M. Ottenheim, and A. F. de Jong, J. Appl. Phys. **70**, 3093 (1991).
[15]Y-H. Hsieh, R. Hull, A. E. White, and K. T. Short, J. Appl. Phys. **70**, 7354 (1991).
[16]R. Hull, Y-H. Hsieh, A. E. White, and K. T. Short, Appl. Phys. Lett. **59**, 3467 (1991).
[17]J. J. Jia, T. A. Callcott, W. L. O'Brien, Q. Y. Yang, D. R. Mueller, J-E. Rubensen, D. L. Ederer, Z. Tan, F. Namavar, and J. I. Budnick, J. Appl. Phys. **69**, 7800 (1991).
[18]S. P. Murarka, *Silicides for VLSI Applications* (Academic, New York, 1983), Chap. IV.
[19]K. N. Tu and J W. Mayer, in *Thin Films—Interdiffusion and Reactions,* edited by J. M. Poate, K. N. Tu, and J. W. Mayer (Wiley, New York, 1978).
[20]E. A. Stern and S. M. Heald, Rev. Sci. Instrum. **50**, 1579 (1979).
[21]E. A. Stern, B. A. Bunker, and S. M. Heald, Phys. Rev. B **21**, 5521 (1980).
[22]J. Mustre, Y. Yacoby, E. A. Stern, and J. Rehr, Phys. Rev. B **42**, 10 843 (1990).
[23]P. Y. Dusausoy, J. Protas, R. Wandji, and B. Roques, Acta Crystallogr. B **27**, 1209 (1971).
[24]U. Birkholz and J. Schelm, Phys. Status Solidi **27**, 413 (1968); **34**, K177 (1969).
[25]Z. Tan, Ph. D. thesis, University of Connecticut, 1990.
[26]K. Radermacher, S. Mantl, Ch. Dieker, and H. Luth, Appl. Phys. Lett. **59**, 2145 (1991).
[27]D. J. Oostra, D. E. W. Vandenhoudt, C. W. T. Bulle-Lieuwma, and E. P. Naburgh, Appl. Phys. Lett. **59**, 1737 (1991).
[28]L. S. Hung, M. Nastasi, J. Gyulai, and J. W. Mayer, Appl. Phys. Lett. **42**, 672 (1983).